Computer modeling and experimental validation of fluorocarbon plasmas applied in the micro-electronics industry

Shu-Xia Zhao

During the period of my Belspo fellowship, i.e., from Oct. 2011 to Dec. 2012, I focused on computer modeling and experimental validation of fluorocarbon (fc) plasmas, which are extensively applied in the micro-electronics industry. The hybrid code, i.e., Hybrid Plasma Equipment Model (HPEM), was used for the modeling work, while the experimental work was conducted by the PSEG group in Dalian University of Technology, who was collaborating with PLASMANT in this period. The ***main objectives of my research*** were:

(1) Ar/CF_4 gas ratio effects on radical species dynamics, electron behavior and Si etching characteristics in an inductively coupled plasma (ICP) reactor,

(2) dissociation and ionization mechanisms in a more complex fc plasma, i.e., C_4F_8, and its dependence on reactor configuration, more specifically ICP and capacitively coupled plasma (CCP) reactor, as well as on the discharge conditions.

These studies help researchers from the micro-electronics industry to understand better the underlying mechanisms of fc plasma sources and the Si-based etching process with fc plasma.

I. INTRODUCTION

To save fabricating costs and to improve the chip properties, the micro-electronics industry is constantly confronted with extremely high criteria for the Si-based etching process with fluorocarbon plasma sources, such as high etching rate, selectivity, anisotropy and high-aspect ratio [1-4]. To achieve this goal, the fundamental fluorocarbon plasma properties need to be explored, including the discharge principles and its interaction with surface materials, for different discharge conditions, reactor configurations and fluorocarbon gases.

In Si-based etching processes, inert gases, such as Ar and He, are typically added to pure fc gases, like CF_4, C_2F_6 and C_4F_8, in order to increase the ion flux towards the wafer, and therefore the etch rate. This process is known as reactive ion etching (RIE), see Fig. 1. The addition of inert gases into a fc plasma can change the chemical components, the electron dynamics and therefore the etching characteristics. Thus, a better insight in the effects of the inert and fc gas mixing ratio on the bulk plasma behavior and the wafer surface kinetics is very important to improve the etching process.
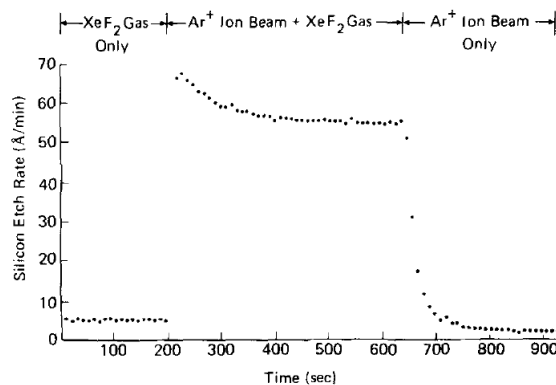
Fig. 1. Ion-assisted gas-surface chemistry using Ar^+ and XeF_2 on silicon[5], illustrating the synergistic effect of mixing an inert gas with a fluorocarbon (or XeF_2) gas, on the Si etch rate.

An inductively coupled plasma (ICP) reactor is characterized by a coil, separated from the reactor by a dielectric window. Radiofrequency (RF) current is flowing through the coil, inducing an electromagnetic field in the plasma reactor. It has many advantages over other reactors, i.e., a simple structure, low pressure and the possibility of separate control over the bulk plasma density (and ion flux) and the ion energy bombarding the wafer [6].Especially the low-pressure makes the ICP reactor the first choice for the Si-based etching industry, since it can generate a highly anisotropic ion flux towards the wafer surface, which results in high-aspect ratio etching, see Fig. 2.
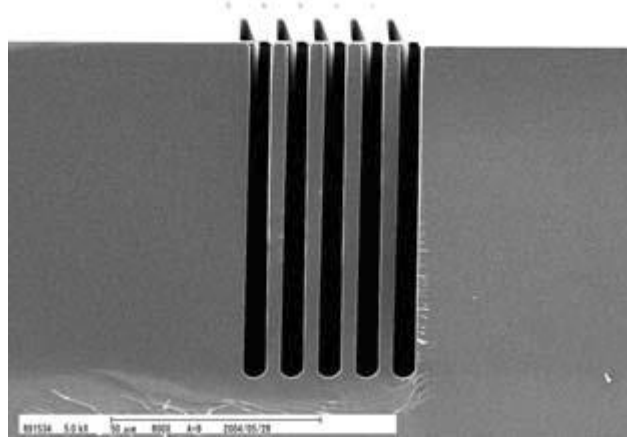
Fig. 2. Illustration of Si-based high-aspect ratio etching by a fc plasma[7]

A capacitively coupled plasma (CCP) reactor, on the other hand, is created by applying a (RF) potential difference between two parallel electrodes in a reactor. It is characterized by a uniform radial profile of the plasma density, at least when the frequency of the applied RF power is not very high[8]. Nowadays, to save manufacturing costs, very-large-dimension (VLD) wafers are proposed. This trend makes CCP reactors also promising for Si-based etching, due to its superiority in spatial uniformity[9].

The main difference between an ICP and CCP is that the plasma in an ICP is sustained by an azimuthal electric field, while in a CCP the plasma is generated by a radial and an axial electric field; see Fig. 3. Hence, even at the same discharge conditions, the fc plasma properties generated in ICP and CCP reactors may be different, and this will influence the etch process.
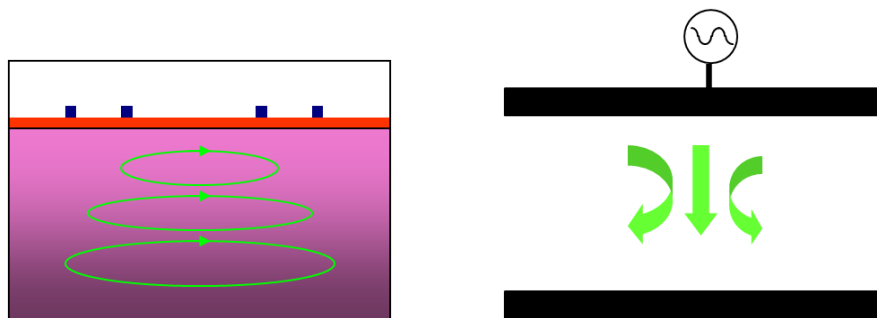
Fig. 3. Different ways of sustaining the plasma by the electric field, an ICP and CCP reactors

The Si-based etching process with fc plasma sources can be understood by four steps, i.e., (1) the formation of a fc polymer film on the wafer surface, (2) the consumption of the polymer by F atoms and ion sputtering, (3) F atoms diffusion through the polymer to fluorinate the Si atoms, and (4) ion sputtering the fluorinated $SiF_{x(x=1-4)}$ layer These four steps are schematically illustrated in Table 1. It is clear that the fc polymer film thickness and uniformity along the wafer surface

critically affects the etch process. Moreover, the polymer layer can also play a role in the selective etching between Si and silicon dioxide (SiO_2) materials due to the thickness difference of the polymers formed at Si and SiO_2 surfaces[10]. Therefore it is very important to study the polymer properties and its effects on the etching characteristics.

Table 1. Four sub-processes of the Si-etching process with a fc plasma[11]

Sub processes	Schematic illustration
Formation of polymer layer on wafer surface	
Consumption of polymer by F atoms and ion sputtering	
F atoms diffusion through the polymer to fluorinate the Si atoms	
Ion sputtering depletion of fluorinated $SiF_{x(x=1,4)}$	
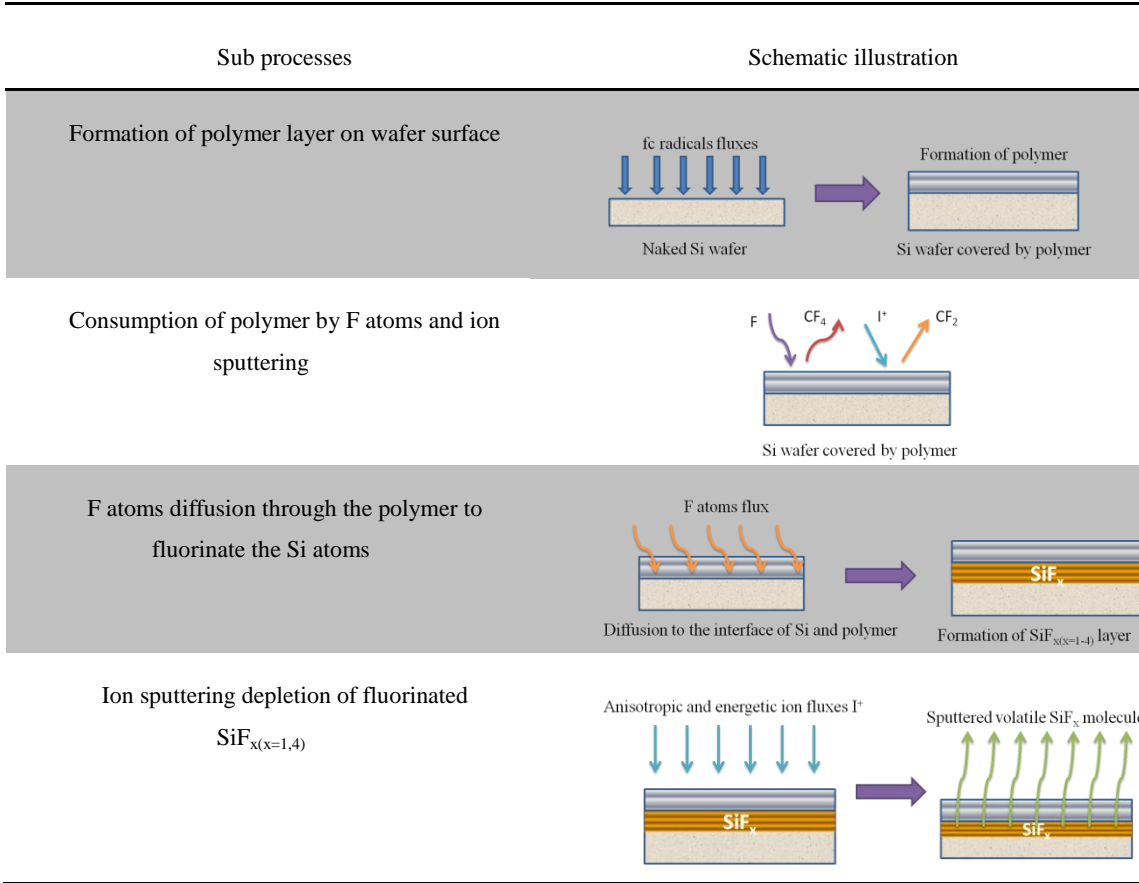
As can be seen from Table.1, the Si-etching process involves F atoms, fc radicals, i.e., CF_2, CF_3, C_2F_4 etc, and high-energy ions, i.e., CF_3^+, $C_3F_5^+$ etc. Therefore, the ratio of these species fluxes to the wafer is very important for the etch characteristics. Moreover, as the various plasma species are mainly formed by dissociation and ionization collisions between electrons and the background fc gas (e.g., CF_4, C_4F_8,…), it is also essential to understand the electron behavior in fc plasmas, since it controls the dissociation and ionization mechanisms and hence the plasma chemical composition, and thus it influences the formed polymer properties and the Si-etching characteristics, as illustrated in Fig. 4.
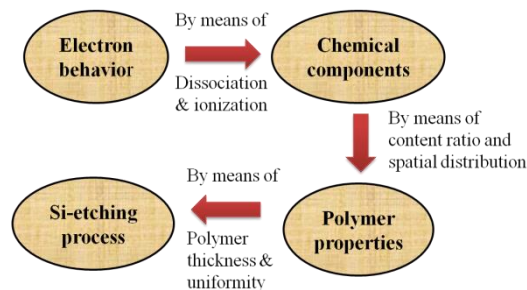
Fig. 4 Schematic of relationship between electron behavior, chemical plasma composition, polymer properties and Si-etching process

During my Belspo fellowship, two main subjects were investigated, i.e., (1) Ar/CF_4 gas ratio effects on the radical

species dynamics, electron behavior and Si etching characteristics in an ICP reactor, and (2) dissociation and ionization mechanisms in a more complex fc plasma, i.e., C_4F_8, and its dependence on reactor configuration, (i.e., ICP and CCP reactor), as well as on the discharge conditions. For this purpose, I made use of the HPEM code for the simulations, which were compared with Langmuir probe measurements at DLUT, to validate the modeling work. The aim of this work was to help researchers in the micro-electronics industry to fully understand the fc plasmas at different conditions, in order to optimize the Si-based etching process.

II. MODEL DESCRIPTION

II.1 Short description of the HPEM code

For the simulations we made use of the HPEM, developed by Kushner and co-workers [12,13]. In this model, the electromagnetic field is calculated based on the Maxwell equations in the so-called electromagnetics module. Subsequently, the field is transferred to the electron Monte Carlo module, which describes the electron dynamics. The rate coefficients of electron impact reactions and the electron temperature are obtained by integrating the calculated electron energy distribution function (EEDF). These quantities are then used as input in the so-called fluid kinetic simulation to generate the densities of charged particles and various radicals by means of continuity equations, as well as the electric field distribution, obtained from the Poisson equation. The electron conductivity, as a function of electron density, is inserted into the electromagnetics module to update the fields. These three modules are solved iteratively until convergence is obtained.

In this work, an extra module, called the surface kinetics module (SKM) [14], was used to address the interaction between bulk plasma and Si wafer surface, and to characterize the process of Si etching and polymer film deposition. The SKM first identifies certain surface locations on the selected materials, initializes the surface species coverage, and extracts reactive and energetic ion fluxes to the surface from the HPEM. Based on a specified surface reaction mechanism, differential equations for the fractional occupancy of surface sites and for the thickness of overlying polymer layers are temporally integrated. After reaching the steady state or a specified computation time, the calculated coefficients, i.e. reflection and sticking coefficients, are transferred back to the HPEM as boundary conditions for solving the gas phase mass and momentum balance equations. The etch rate and deposited film thickness are obtained based on the surface coverage and reactive fluxes, as calculated in SKM.

II.2 Gas-phase reaction set

Gas-phase reaction sets were built for Ar/CF_4 and C_4F_8 plasmas. The considered species for the Ar/CF_4 gas mixture are listed in Table 2. For all these species, surface reaction coefficients, i.e., sticking, reflection, neutralization and recombination) were introduced in the model, to determine their boundary conditions at the reactor walls, as well as the Si wafer etch process. Besides, a list of all possible reactions that can occur between these species, including electron-impact reactions, i.e., ionization, dissociation, excitation and attachment, as well as reactions among the heavy species, i.e., atom and charge exchange, de-excitation and Penning ionization, was constructed, along with the corresponding cross sections and rate coefficients. This complete list was presented in the Mid-Term report of this fellowship, and can also be found back in our recent papers[15,16].

Table 2. Species included in the model for the Ar/CF$_4$ gas mixture, besides the electrons

Molecules	Charged species	Radicals	Excited species
Ar, F$_2$, CF$_4$	e$^-$, Ar$^+$, CF$_3^+$, CF$_2^+$, CF$^+$, F$^+$, F$_2^+$, CF$_3^-$, F$^-$	CF$_3$, CF$_2$, CF, F, C	Ar*, F*

Table 3. Species included in the model for the C$_4$F$_8$ gas, besides the electrons

Type	Species
C species	C, C$^+$
F species	F, F$^-$, F$^+$, F$_2$, F$_2^+$
CF$_x$ species	CF, CF$_2$, CF$_3$, CF$^+$, CF$_2^+$, CF$_3^+$
C$_x$F$_y$ species	C$_2$F$_3$, C$_2$F$_4$, C$_2$F$_5$, C$_2$F$_6$, C$_3$F$_5$, C$_3$F$_6$, C$_3$F$_7$, C$_4$F$_8$, C$_4$F$_8^-$, C$_4$F$_8^{*-}$, C$_2$F$_3^+$, C$_2$F$_4^+$, C$_2$F$_5^+$, C$_3$F$_5^+$, C$_3$F$_6^+$, C$_3$F$_7^+$, C$_4$F$_7^+$

The C$_4$F$_8$ reaction set is much more complicated, since one C$_4$F$_8$ molecule has 4 C atoms and 8 F atoms. The fragmentation of C$_4$F$_8$ can be diverse, and hence the C$_4$F$_8$ plasma contains light (i.e., CF$_x$ and CF$_x^+$), middle (i.e., C$_2$F$_x$ or C$_2$F$_x^+$) and heavy (i.e., C$_4$F$_x$ or C$_4$F$_x^+$) fc radicals and ions. The species considered in the model for the C$_4$F$_8$ plasma are presented in Table 3. Again, for all these species the corresponding surface reaction coefficients and the collision processes in the plasma were specified. Since the complete reaction set is too long to be presented in this report, only an overview of the electron-impact reaction scheme is given in Fig. 5. More details will be presented in a forthcoming paper.
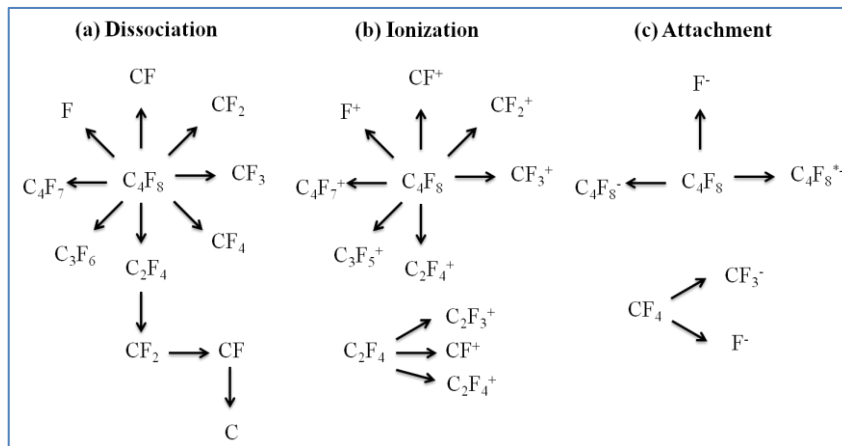
Fig. 5. Schematic picture of the electron-impact reaction set occurring in the C$_4$F$_8$ plasma: (a) dissociation, (b) ionization and (c) attachment, including the precursor molecule and its fragmented species.

II.3 Wafer surface reaction kinetics

The main surface mechanisms occurring in a fc plasma are listed in Table 5. They include polymer growth by C$_x$F$_y$ radicals (mainly CF$_2$) (a), polymer depletion by F atom etching (b) and by ion sputtering (c), fluorination of Si by F atoms, gradually forming SiF$_{x(x=1-4)}$ (d), and etching of fully fluorinated Si sites (SiF$_4$) by ion sputtering (e). Besides, it is well known from experiments that the etching of Si by ion sputtering can happen underneath the polymer, which is formed on top of the Si surface. Thus it is believed that there should be a diffusion mechanism of the Si etching precursor, i.e., F atoms, from the formed polymer layer surface towards the interface of this layer with the Si surface. Therefore, in our surface

model, three additional sub-processes are included, i.e., F atom accumulation at the top of the polymer when the Si surface is covered by polymer (f), F atom accumulation at the top of the Si surface when the Si surface is still naked (g), and finally diffusion of F atoms collected above the polymer surface towards the interface between polymer and Si surface (h). The definition of the surface site quantities is given in Table 6. More explanation about this surface mechanism can be found in our paper [16].

Table 5. Main Si etching and polymer deposition mechanisms, and the corresponding surface reactions.

Reaction type	Chemical reaction
(a) Polymer formation	(1) $CF_2 + S_{Poly} \rightarrow Poly$
	(2) $CF_2 + Poly \rightarrow 2Poly$
(b) Polymer consumption by attached F atoms	(3) $F_{Poly}(A) + Poly \rightarrow CF_4 + S_{Poly,F}$
(c) Polymer consumption by ion sputtering	(4) $Ar^+ + Poly \rightarrow Ar + CF_2$
	(5) $CF_3^+ + Poly \rightarrow CF_3 + CF_2$
(d) Fluorination of Si and SiF_x	(6) $F_{Si}(A) + SiF_x(s) \rightarrow SiF_{x+1}(s)$ (x=0-3)
(e) Ion sputtering of volatile SiF_4	(7) $Ar^+ + SiF_4(s) \rightarrow Ar + SiF_4$
	(8) $CF_3^+ + SiF_4(s) \rightarrow CF_3 + SiF_4$
(f) F atom accumulation at the top of the polymer	(9) $F + S_{Poly,F} \rightarrow F_{Poly}(A)$
(g) F atom accumulation at the top of the Si surface	(10) $F + S_{Si,F} \rightarrow F_{Si}(A)$
(h) F atom diffusion from the polymer top to the Si surface	(11) $F_{Poly}(A) + S_{Si,F} \rightarrow F_{Si}(A) + S_{Poly,F}$

Table 6. Surface site quantities, as defined in our model

Symbol	Description
Poly	Polymer layer
$S_{Poly,F}$	Artificial layer representing the top of the polymer, available for F atom accumulation
S_{Poly}	Artificial layer used for polymer growth
$S_{Si,F}$	Artificial layer representing the top of Si, available for F atom accumulation
$F_{Poly}(A)$	F atoms accumulated on top of the polymer layer
$F_{Si}(A)$	F atoms accumulated on top of the Si surface
Si(s)	Fraction of pure Si surface sites
$SiF_x(s)$	Fraction of fluorinated Si surface sites by x F atoms (x=1-4)

III. EXPERIMENTAL SETUP

The experimental ICP setup is schematically shown in Fig. 6. The reactor consists of two parts, i.e., the upper discharge vacuum chamber (28 cm in diameter and 25 cm in height) and the lower vessel (30 cm in diameter and 21 cm in height). An aluminum substrate of 15 cm in diameter is fixed at a distance of 11 cm from the top of the upper chamber. A 13.56 MHz RF power is connected to a two-turn planar coupling coil via a Γ-type matching network. The coil is located above a quartz window which is mounted on top of the discharge vacuum chamber. The applied power P_a is determined from the source forward power minus the reflected power, both measured by the power supply meter. The substrate can also be connected to an RF power source by a matching network, but in the present work it is grounded. Two mass flow controllers are used to control the flow rates of CF_4 and Ar, respectively. The total flow rates were fixed at 50 sccm (standard cubic centimetres per minute). A mechanical pump (8 L/s) and a turbine molecular pump (400 L/s) are used to evacuate the reactor, and the base

pressure of the chamber is 1.5×10^{-3} mTorr.

Langmuir probe measurements are performed on this reactor, to validate the model results. The Langmuir probe (Hiden Analytical Ltd) is fixed at about the centre of the discharge to measure the electron density, electron temperature and EEDF. The probe tip (10 mm long and 0.2 mm in diameter) is made of a platinum wire. The current-voltage (I-V) characteristic curve of the probe is measured by sweeping the voltage on the probe from -20 to +30 V. These data are recorded by a pc. From the I-V curve, the electron density, temperature and EEDF can be derived [8]. We refer to refs. 28 and 29 for more details about the ICP experimental setup and measurements.
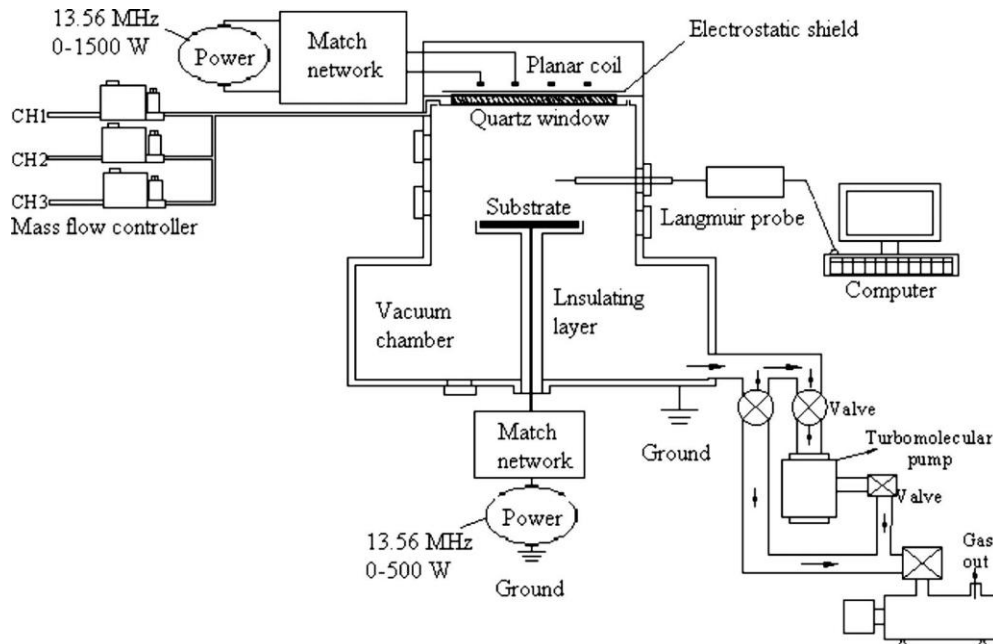
Fig. 6 Schematic diagram of the planar-type ICP reactor used in the experiment

IV. RESULTS AND DISCUSSION

In this section, four different types of results will be presented: (a) the chemical composition of the Ar/CF$_4$ plasma and the spatial characteristics of the important gas-phase species in the ICP reactor, versus CF$_4$/(Ar+CF$_4$) content ratio, (2) the effects of F$_2$ attachment with low-energy electrons on the electron behavior in a ICP operating also in an Ar/CF$_4$ gas mixture, (3) the gas ratio effects on the Si-etching process in an ICP operating again in the Ar/CF$_4$ mixture, and (4) the dissociation and ionization mechanisms of a C$_4$F$_8$ plasma and its dependence on the discharge conditions and reactor configuration. The results of parts (a-c) were (partly) presented in [15,16]. The results of part (d) will be used for a forthcoming paper (still in preparation).

IV.1 Chemical composition and spatial characteristics of a Ar/CF$_4$ plasma

The gas ratio effects on the density magnitudes and on the spatial profiles of important species, which are either mainly fragmented (i.e., CF$_3$) or Si-etching process related (i.e., F), as well as of the electrons (e$^-$) which play a very important role in creating the reactive plasma species, will be presented here for the ICP reactor, for various CF$_4$ contents. The discharge conditions are an ICP power of 400W, a gas pressure of 30mT, and a total gas flow rate of 30sccm.

The F density profile at low CF$_4$ content, i.e., 10%, is plotted in Fig. 7(a). It is mainly determined by the pumping loss [18] at the bottom edge of the chamber, so it is characterized by a maximum near the gas inlet (top center of the reactor) and

a gradual drop in density towards the pump position.. However, at high CF_4 contents, i.e., 50% and 80%, the maximum F density shifts from the center towards the position under the coil, as shown in Fig. 7(b) and (c). This indicates that the profile is mainly determined by the F atom generation source, i.e., $e^- + CF_4 \rightarrow CF_3 + F + e^-$, which is at maximum underneath the coil. The F density magnitude increases with CF_4 content, in the low CF_4 content range, i..e, from 10% to 50%, due to the higher density of CF_4 molecules. However, in the higher CF_4 content range, i.e., from 50% to 80%, the F density hardly changes with CF_4 content. This is caused by the competition between the increasing CF_4 source and the decreasing electron source upon increasing CF_4 content; see the electron density profiles in Fig. 9 below.

The CF_3 radical density is plotted for the same conditions in Figure 8. It shows the same trends against CF_4 content as the F atoms, i.e., with a maximum near the gas inlet and gradually dropping towards the pump port at low CF_4 content (i.e., 10%; see Fig. 8(a)), and with a maximum localized under the dielectric window at higher CF_4 content, -, as shown in Fig. 8(b) and (c). Also the change in density values is similar as for the F atoms, with an increase in the lower CF_4 content range, and more or less constant values in the higher CF_4 content range.

The electron density increases with increasing CF_4 content, at low CF_4 content values, but it drops again slightly in the higher CF_4 content range, as shown in Fig. 9(a)-(c). Meanwhile the density profile becomes more localized under the dielectric window and the density peak shifts from the discharge center to the dielectric window. This change of electron density profile explains the   the spatial characteristics and density values of the important chemical plasma species, like F and CF_3.
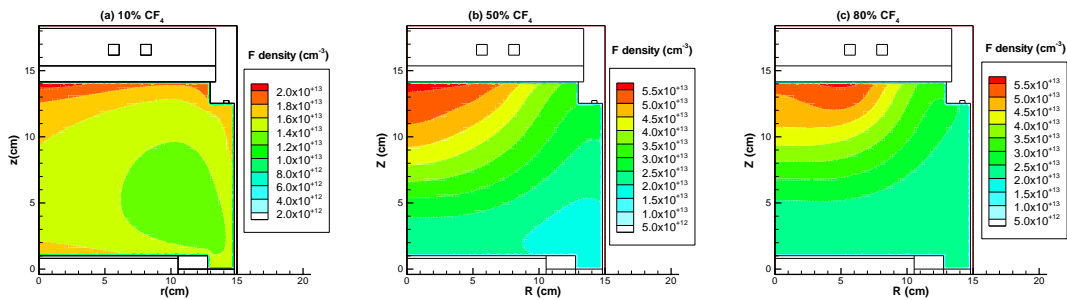
Fig. 7. F density profiles in the ICP reactor for different CF_4 contents, i.e., (a) 10%, (b) 50% and (c) 80%. The other discharge conditions are as follows: an ICP power of 400W, a gas pressure of 30mT, and a gas flow rate of 30sccm. Note that only one half cross-section of the cylindrically symmetrical ICP reactor is shown. The gas inlet is at the top center (r=0 cm), the coil is at the top, the wafer is at the bottom, and the pump port is also at the bottom, next to the wafer.
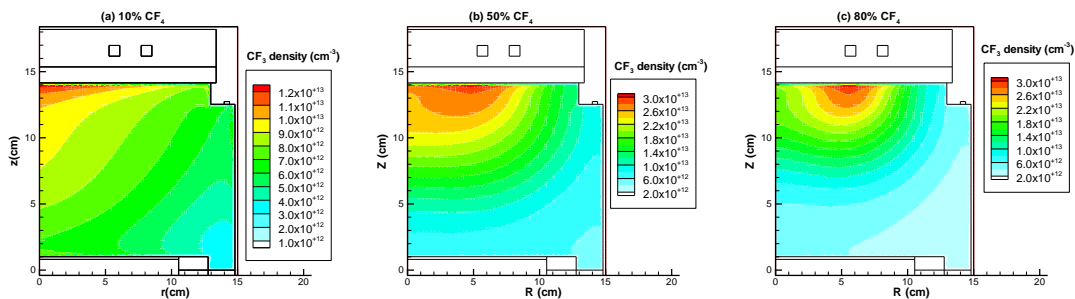
Fig. 8 CF_3 density profiles in the ICP reactor for different CF_4 contents, i.e., (a) 10%, (b) 50% and (c) 80%, for the same discharge conditions as in Fig. 7.
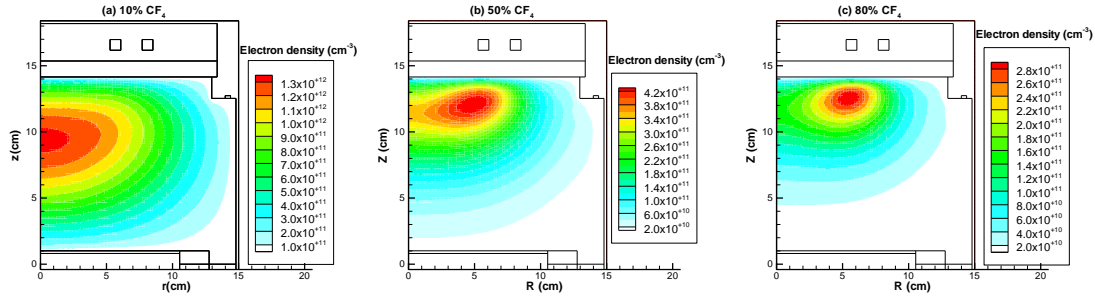
Fig. 9 Electron density profiles in the ICP reactor for different CF_4 contents, i.e., (a) 10%, (b) 50% and (c) 80%, for the same discharge conditions as in Fig. 7.

IV.2 Effect of F_2 attachment by low-energy electrons on the electron behavior in an ICP Ar/CF_4 plasma

The electron density n_e and the electron temperature T_e, measured at the reactor centre by the Langmuir probe (i.e. at the radial axis: $r = 0$ cm, and at 7.0 cm above the substrate) are presented in Figs. 10 and 11, for different values of CF_4 content in the gas mixture, gas pressure and coil power. It is clear from Fig. 10 that the electron density n_e decreases significantly with increasing CF_4 content, i.e. the density at 10% of CF_4 is typically about three times lower than in the pure Ar plasma. This trend of decreasing density is quite similar for the different values of power investigated (see Fig. 10(a)), but at high pressure, i.e. 30mTorr, the drop is somewhat more pronounced than at low pressure, i.e. 10mTorr (see Fig. 10(b)).

The measured T_e values upon increasing CF_4 content are plotted for different values of power and pressure in Fig. 11. In all cases, T_e rises with CF_4 content, but the slope changes upon increasing CF_4 fraction, i.e. a large increase is observed when a small amount of CF_4 gas (~1%) is added, but at higher CF_4 fractions, i.e. $\geqslant 2\%$, the increase is not so pronounced. The trend of increasing T_e upon increasing CF_4 fraction is almost the same for the different values of pressure and power investigated.
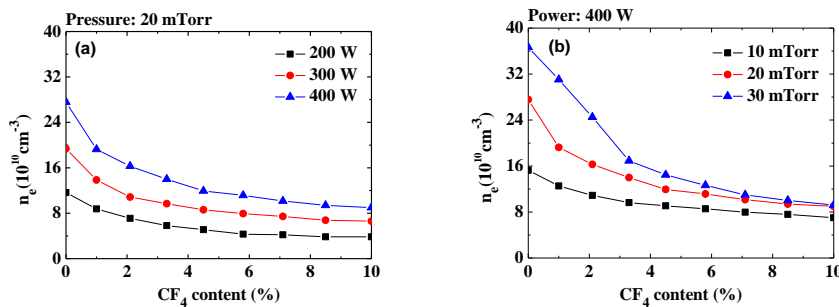
Fig. 10 Experimentally measured electron densities at the reactor center (i.e., radial axis: r=0 cm, and at 7.0 cm above the substrate) versus CF_4 content in the Ar/CF_4 mixture, for different values of (a) coil power (at a pressure of 20 mTorr) and (b) gas pressure (at a coil power of 400 W).
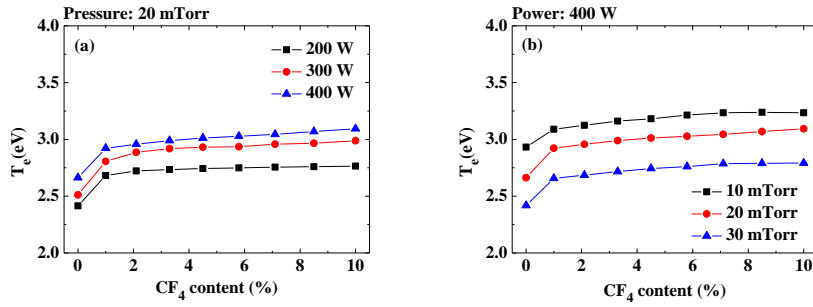
Fig. 11 Experimentally measured electron temperatures at the reactor center versus CF_4 content in the Ar/CF_4 mixture, for different values of (a) coil power (at a pressure of 20 mTorr) and (b) gas pressure (at a coil power of 400 W).

Two sets of calculations have been carried out, i.e. with two different boundary conditions for the F atoms, i.e., called bcI (i.e., stuck F atoms will be released as F_2 upon impact of a second F atom) and bcII (where the majority of F atoms is just reflected), as explained in Table. 7. The calculated electron density and temperature (obtained at the same position as in the experiment, i.e. at the radial axis and at a distance of 7.0 cm above the substrate) at a coil power of 400W and a gas pressure of 10mTorr, are plotted versus CF_4 content in the gas mixture in Fig. 12, for these two different boundary conditions. It is clear from Fig. 12(a) that the electron density calculated with bcI decreases more drastically than with bcII. Similarly, the rise in electron temperature with increasing CF_4 content, illustrated in Fig. 12(b), is predicted to be much more pronounced with bcI than with bcII. Obviously, the modelling predictions obtained with bcI are in much better agreement with experiment than the results obtained with bcII, at least qualitatively.

Table. 7 Sticking coefficients assumed for the various radicals used in the model[15]

Species	CF_3	CF_2	CF	F (bcI)[a]	F (bcII)[b]	C
Sticking coefficient	0.012	0.014	0.048	0.5	0.0048	1

[a]The F atom sticking coefficient is 0.5 and all stuck F atoms are recombined with each other along the surface and then reflected back into the plasma as F_2 molecules.

[b]The F atom sticking coefficient is low, i.e., 0.0048, and the stuck F atoms are consumed at the surface.

The 2D profiles of the F_2 molecule density obtained with bcI and bcII, at a CF_4 content of 10%, are shown in Fig. 13. It is clear that the F atom recombination at the reactor walls significantly affects the F_2 density profile. Indeed, the density obtained with bcI (i.e., stuck F atoms will be released as F_2 upon impact of a second F atom) is two orders of magnitude higher than for bcII (where the majority of F atoms is just reflected).
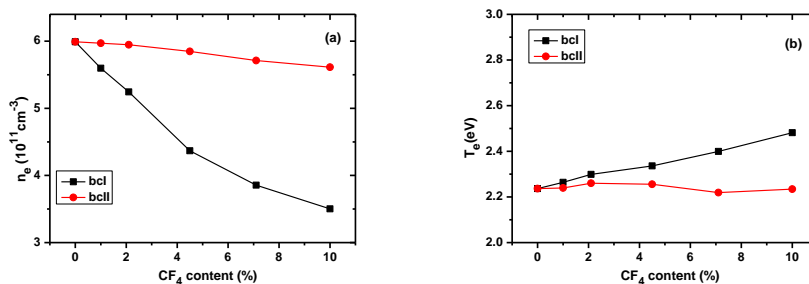
Fig. 12 Calculated electron density (a) and temperature (b) versus CF_4 content in the Ar/CF_4 mixture, obtained at the same position as in the experiments (i.e., at the reactor center and at a distance of 7.0 cm above the substrate), assuming two different boundary conditions for the F atoms, as explained in the text. The coil power and the gas pressure are 400 W and

10 mTorr.
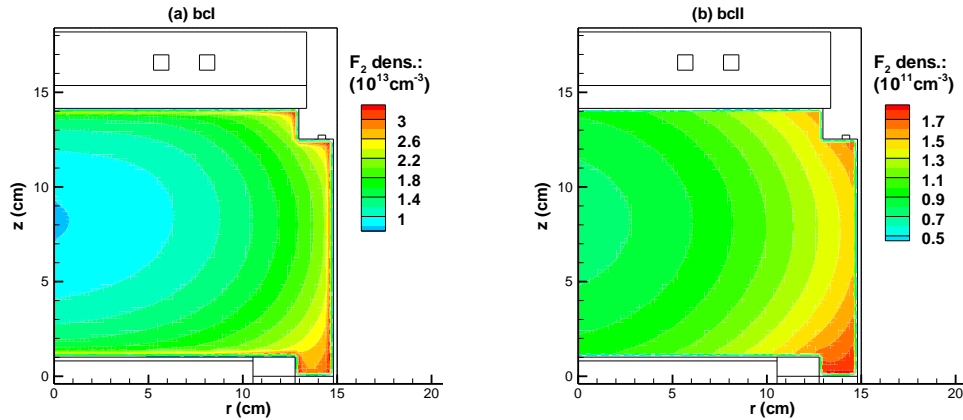
Fig. 13 Calculated F_2 molecule density profiles, obtained with bcI (a) and bcII (b), at a coil power of 400 W and a gas pressure of 10 mTorr. The CF_4 content is 10%.
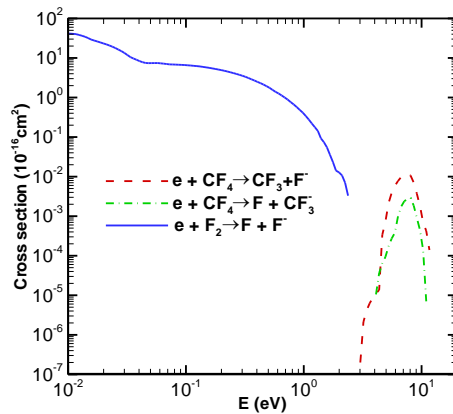
Fig. 14 Electron attachment cross sections with CF_4 and F_2 as a function of electron energy.

To investigate the role of F_2 molecules in the electron behaviour, the cross sections of electron attachment with both CF_4 and F_2 are plotted vs. electron energy in Fig. 14. The cross section for electron attachment with F_2 is several orders of magnitude higher than for attachment of CF_4, and moreover, it is significant in the low energy region. Therefore, we believe that electron attachment of F_2 may consumes a large fraction of low-energy electrons, and this might explain the significant drop in electron density, and the increase in electron temperature, upon addition of CF_4 to the Ar/CF_4 gas mixture. These findings were published in [15].

IV.3 Gas ratio effects on Si-etching uniformity in an ICP with Ar/CF_4 mixture, and role of the polymer layer

Information on the polymer formation at the wafer surface, i.e., number of monolayers formed and the polymer thickness, as well as the etch rate along the wafer radius at 10%, 50% and 90% CF_4 contents are presented in Fig. 15. It can be seen from Fig. 15 (a) that typically a few monolayers are formed, corresponding to a thickness of a few nm. The polymer film is thicker at high CF_4 contents, which is like expected, because it gives rise to more CF_2 species, which are the main precursors for the polymer growth. Meanwhile the radial uniformity of the layer along the wafer is reduced. This will be explained below. The presence of the polymer layer affects the etching characteristics significantly. More specifically, the

etch rate is significantly reduced, as shown in Fig. 15 (b). Besides, the radial uniformity of the etch rate is also worse at high CF_4 content, following the pattern of the polymer thickness.
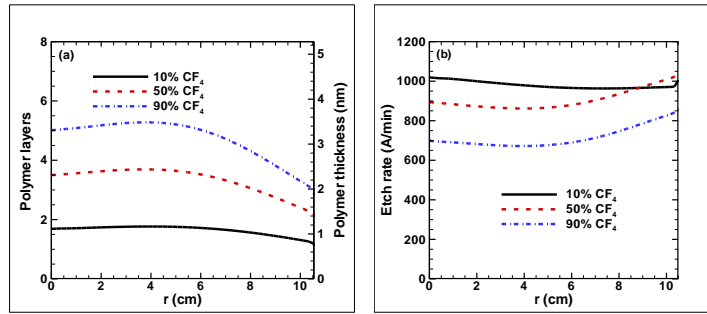
Fig. 15 Calculated polymer thickness (in number of layers and in nm) (a) and etch rate (b), along the wafer radius, at 10%, 50% and 90% of CF_4 content. The power and pressure are 500 W and 10 mTorr, respectively. The substrate is radio frequency (rf) biased by a 100 V voltage source. The frequencies for the coil and substrate sources are both 13.56 MHz.
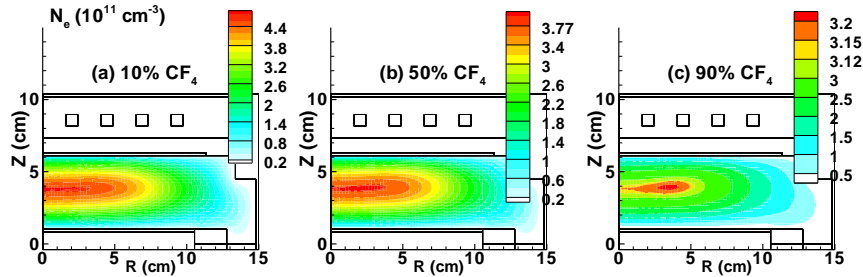
Fig. 16 Electron density profiles at (a) 10%, (b) 50% and (c) 90% of CF_4 content, for the same conditions as in Fig. 15.
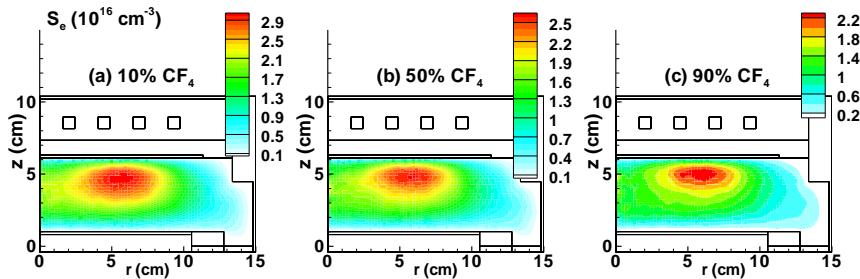
Fig. 17 Electron impact ionization rate profiles, summed over both Ar and CF_4, at (a) 10%, (b) 50% and (c) 90% CF_4 content, for the same conditions as in Fig. 15.

The non-uniformity of the polymer can be explained by looking at the electron density profiles at 10%, 50% and 90% CF_4 content in Fig. 16. At 10% CF_4 content, the electron density reaches a broad maximum in the center, up to 5 cm from the discharge axis, and then drops gradually by a factor of 2 towards the end of the wafer, whereas at 90% CF_4 content, the density is less uniform, with a peak off-axis, and a drop in the radial direction by a factor of 3 over a shorter distance. The electron density distribution clearly affects the radial distribution in the CF_2 density and flux. Indeed, the CF_2 radicals are mainly produced by electron impact dissociation.

To explain the radial non-uniformity of the electron density, we need to investigate their production and loss processes. Fig. 17 shows the total electron impact ionization rate profiles at 10%, 50% and 90% CF_4 content. Indeed, electron impact ionization is the main production process for the electrons. The ionization rate always exhibits a maximum under the quartz window at about 6 cm away from the axis, so this cannot explain the radial non-uniformity of the electron density. Therefore,

the latter needs to be explained by the loss mechanisms. At high CF_4 contents, more fluorocarbon neutrals, i.e., CF_4, CF_3, CF_2, F and F_2, are present in the discharge, and they can all consume electrons by means of electron (dissociative) attachment. At low CF_4 contents, e.g., 10%, when less fluorocarbon species are present, the amount of electrons depleted is small and the electron diffusion mechanism from the ionization source can balance the electron loss scheme through electron attachment of various CF_x species. Therefore, the electron density profile is rather uniform, like in a pure Ar plasma, as seen from Fig. 17 (a). However, at high CF_4 contents, when the fluorocarbon neutrals are quite abundant, the electron loss by attachment is much more important, and the balance between the electron diffusion mechanism and electron loss by attachment, necessary for maintaining a uniform and center-peaked plasma density profile, is broken. Therefore, the electron density peak moves away from the discharge center and exhibits a maximum at about 4 cm away from the axis, showing a more localized and less uniform profile (see Fig. 17 (c)). Hence, this behavior can explain the polymer thickness and etch rate along the wafer radius. More details about this investigation can be found in [16].

IV.4 Dissociation and ionization mechanism of C_4F_8 plasma in ICP and CCP reactors
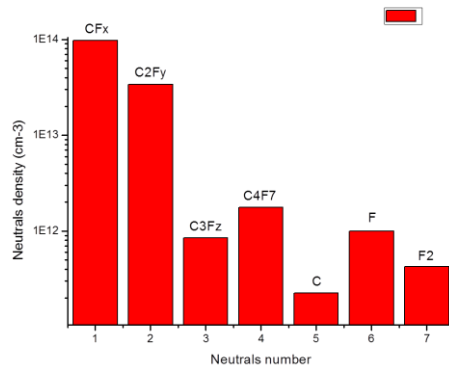
Fig. 18. Density of various neutrals, i.e., CF_x, C_2F_y, C_3F_z, C_4F_7, C, F, F_2, in a C_4F_8 ICP reactor, averaged over the reactor geometry. The coil power and gas pressure are 500 W and 10 mTorr. The frequency of the power source is 13.56MHz, and the gas flow rate is 30 sccm.

(a)   (b)
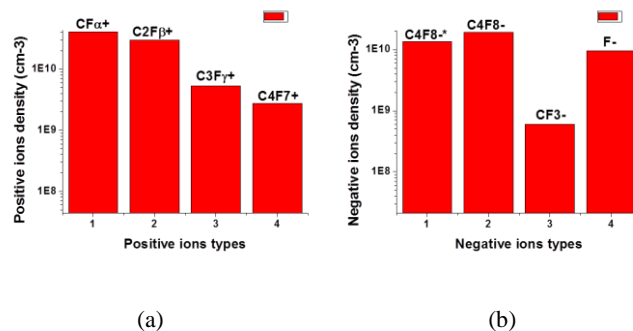
Fig. 19 Density of various positive ions (a) i.e., CF_α^+, $C_2F_\beta^+$, $C_3F_\gamma^+$, $C_4F_7^+$, and negative ions (b) , i.e., $C_4F_8^{-*}$, $C_4F_8^-$, CF_3^-, F^-, in a C_4F_8 ICP reactor, averaged over the reactor geometry. The discharge conditions are the same as in Fig. 18.

In Figs. 18 and 19, the densities of various neutral species and (positive and negative) ions are presented, illustrating the total dissociation and ionization status of the C_4F_8 ICP. The discharge conditions are as follows. The coil power and the gas pressure are 500 W and 10 mTorr. The frequency of the power source is 13.56MHz, and the gas flow rate is 30 sccm.

The main neutrals are classified into 7 types, i.e., CF_x, C_2F_y, C_3F_z, C_4F_7, C, F, F_2. Here CF_x means the sum of CF, CF_2 and CF_3. C_2F_y means the sum of C_2F_3, C_2F_4 , C_2F_5, and C_2F_6. C_3F_z means the sum of C_3F_5, C_3F_6 , and C_3F_7. It can be seen from Fig. 18 that the CF_x radicals have the highest density in the plasma, at the conditions under study.

In fc plasmas, positive ions are generated mainly by electron-impact ionization or dissociative ionization, and the negative ions are generated mainly by electron attachment or dissociative attachment, as shown in Fig. 5. In Fig. 19, both positive and negative ions are plotted to examine the ionization and attachment mechanisms in the C_4F_8 ICP reactor. Again, the main positive ions are lumped as CF_α^+, $C_2F_\beta^+$, $C_3F_\gamma^+$, $C_4F_7^+$, where CF_α^+ means the sum of CF^+, CF_2^+ and CF_3^+, $C_2F_\beta^+$ is the sum of $C_2F_3^+$, $C_2F_4^+$ and $C_2F_5^+$, $C_3F_\gamma^+$ is the sum of $C_3F_5^+$, $C_3F_6^+$ and $C_3F_7^+$. It can be seen from Fig. 19(a) that the CF_α^+ ions are again the most important species at the conditions under study. This behavior corresponds to experimental data [19] under similar discharge conditions. As for the negative ions, $C_4F_8^-$, which is generated by direct attachment of electrons with C_4F_8, is found to be the most important type of negative ions.
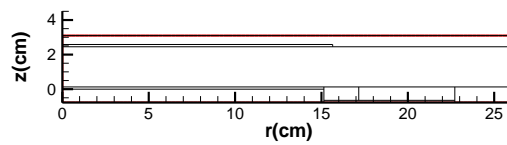
Fig. 20. Schematic picture of the CCP reactor assumed in the model. A shower head is fixed underneath the top electrode. The pump is fixed at the bottom edge of the chamber.

Fig. 20 illustrates the CCP reactor used in the simulations. Calculations were performed for the following conditions: The bottom electrode is powered by a 27.12MHz source. The applied power and the gas pressure are 500 W and 10 mTorr, respectively. The gas flow rate is 100sccm. Figs. 21 and 22 present the densities of the various radicals, positive and negative ions in the C_4F_8 CCP reactor. The same species are listed in in the ICP reactor. It can be seen from Fig. 21 that now the C_2F_y radicals are the most important species in the CCP reactor. As for the ions, we can see from Fig. 22(a) that both $C_2F_\beta^+$ and $C_3F_\gamma^+$ are now the most important positive ions. For the negative ions, Fig. 22(b) demonstrates that both the excited negative ions $C_4F_8^{*-}$ and the light F^- ions (which are generated by dissociative attachment) are the most important species. When comparing these results with the ICP model results, it can be concluded that the main chemical components are greatly dependent on the reactor configuration (ICP vs CCP). This information is very important for the micro-electronics industry, as the chemical composition in the plasma will affect the etching characteristics.
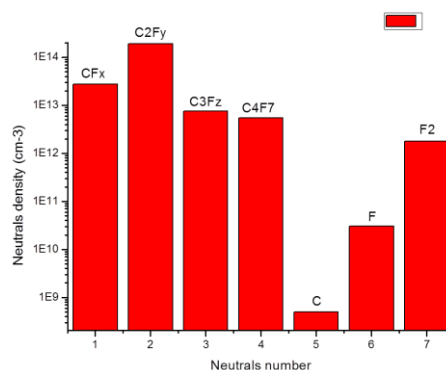
Fig. 21 Density   of various neutrals, i.e., CF_x, C_2F_y, C_3F_z, C_4F_7, C, F, F_2, in the C_4F_8 CCP reactor, averaged over the reactor geometry. The discharge conditions are specified in the text.
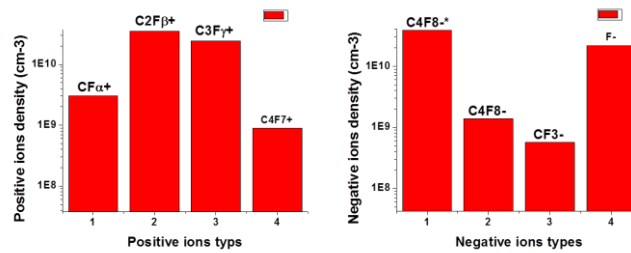
Fig. 22 Density of various positive ions (a) i.e., CF_α^+, $C_2F_\beta^+$, $C_3F_\gamma^+$, $C_4F_7^+$, and negative ions (b) , i.e., $C_4F_8^{-*}$, $C_4F_8^-$, CF_3^-, F^-, in the C_4F_8 CCP reactor, averaged over the reactor geometry. The discharge conditions are specified in the text.

V. CONCLUSION

During this Belspo fellowship, I focused on computer modeling and experimental validation of different fc plasmas used for the micro-electronics industry. The HPEM code was used for the simulations, whereas a Langmuir probe was applied for the experimental vallidation. The main objectives of my work included the study of (1) Ar/CF$_4$ gas ratio effects on radical species dynamics, electron behavior and Si etching characteristics in the ICP reactor, and (2) dissociation and ionization mechanisms in a more complex fc plasma, i.e., C_4F_8, and its dependence on reactor configuration, i.e., ICP and CCP reactor. These studies help researchers from the micro-electronics industry to understand better the underlying mechanisms of fc plasma sources and the Si-based etch process with a fc plasma.

References

[1]H. Rhee et al, J. Vac. Sci. Technol. B 27, 33 (2009)

[2]M. Sekine, Appl. Surf. Sci. 192, 270 (2002)

[3]H. Motomura, Thin Solid Films, 390, 134 (2001)

[4]A. Sankaran and M. J. Kushner, Appl. Phys. Lett. 82, 1824 (2003)

[5]J. W. Coburn and H. F. Winters, J. Appl. Phys. 3189, 50 (1979)

[6]A. Maresca et al, Phys. Rev. E, 65, 056405 (2002)

[7]S. Aachboun and P. Ranson , J. Vac. Sci. Tech. A, 2270, 17 (1999)

[8]A. V. Vasenkov and M. J. Kushner, J. Appl. Phys., 95, 834 (2004)

[9]K. Ellinas et al, Microelectronics Engineering, 88, 2547 (2011)

[10]K. H. R. Kirmse et al, J. Vac. Sci. Technol. B, 14, 710 (1996)

[11]D. Zhang and M. J. Kushner, J. Appl. Phys., 87, 1060 (2000)

[12]M. J. Kushner, J. Phys. D: Appl. Phys., 42, 194013 (2009)

[13]Y. Yang and M. J. Kushner, Plasma Sources Sci. Technol., 19, 055011 (2010)

[14]D. Zhang and M. J. Kushner, J. Vac. Sci. Technol. A, 18, 2661 (2000)

[15]S. X. Zhao et al, Plasma Sources Sci. Technol., 22, 025008 (2012)

[16]S. X. Zhao et al, Plasma Sources Sci. Technol., 22, 015017 (2013)

[17]A. V. Vasenkov et al, J. Vac. Sci. Technol. A 22, 511 (2004)

[18]H. Hayashi H et al, J. Vac. Sci. Technol. A, 17, 2557 (1999)

[19]X. Li et al, J.Vac. Sci. Technol. A, 22, 500 (2004)